Angewandte Chemie
Eine Zeitschrift der Gesellschaft Deutscher Chemiker

Supporting Information

69451 Weinheim, Germany

A pocket-sized convective PCR thermocycler

Nitin Agrawal, Yassin A. Hassan, and Victor M. Ugaz

Additional notes on device construction and assembly

Assembly of the convective thermocycling devices involves (1) loading the flow loops with PCR reagents and (2) mounting the loops on the heater assembly. The loading process begins by cutting appropriate lengths of tubing. In the triangular geometry shown in Supplementary Figure 4a, the flow loop is constructed using an 8.75 cm length of FEP tubing and a 1 cm length of Tygon tubing. We typically use 0.01 and 0.02 inch inside diameter Tygon tubing (Small Parts Inc, Catalog # TGY-010 and TGY-020 respectively, depending on the outside diameter of the corresponding FEP tubing) so that the end of the FEP segment will fit snugly inside the flexible Tygon segment. One end of the FEP segment is then inserted into one end of the Tygon segment, after which the assembled length of tubing is rinsed in DI water and allowed to air dry. Next, the tubing is bent into a U-shape and held in one hand while an appropriate volume of PCR reagent mixture is pipetted into the Tygon end until a convex meniscus forms at both ends. The free end of the FEP segment is then brought into contact with and inserted into the free end of the Tygon segment and secured tightly to obtain a 9 cm long closed loop reactor (Supplementary Figure 4b). It is important to make sure that no air pockets are present inside the loop, particularly in the vicinity of the FEP/Tygon junction, because they may expand upon heating and distort the flow field. The assembled loop can then be loaded onto the thermocycling apparatus.

The loading process involves inserting the tubing around the scaffold with the Tygon segment at the bottom of the triangular loop (more than one loop can be loaded at once to run multiple reactions). Next, a piece of aluminum PCR sealing tape is cut wide enough to cover all the tubes and long enough to extend over all three sides of the loop. The tape is then used to adhere the tubing segments against the heated surfaces on all three sides of the loop, taking care to press down firmly (e.g., with the blunt end of a paintbrush) around the tubing on all sides in order to ensure good thermal contact. The outside of the loops are then covered with a strip of ceramic fiber cloth that is secured by clamping the ends together at the bottom of the triangle using a binder clip. This arrangement minimizes the effects of ambient temperature fluctuations to ensure temperature uniformity throughout the run, as was evident in our ability to regulate the thermoelectric heaters with +/– 0.3 °C accuracy by manually adjusting the applied voltage.

A similar process is used to load the battery powered device, except that shorter lengths of tubing are employed. Photographs of each device after loading a loop of tubing but prior to securing them with the aluminum tape and insulation are shown in Supplementary Figure 4. After the reaction is complete, the loops are removed and opened so that the products can be aspirated from one end of the tubing segment using a pipettor.

The pocket-sized thermocycler incorporates a design whereby three aluminum blocks are interconnected in a way that enables the heat flow between them to be regulated. We demonstrate this concept by simply using screws of different thermal conductivity to join the blocks (Supplementary Figure 4c,d). Here, three nominal thread sizes (0-80, 1-72 and 2-56) of stainless steel machine screws (Small Parts Inc. Catalog # B-MX-080-6, B-MX-172-6 and B-MX-256-6 respectively) are used to connect the denaturing and extension zones, while two nominal thread sizes (2-56 and 0-80) of nylon machine screws (Small Parts Inc. Catalog # B-

MN-256-6F and B-MN-172-6F respectively) are used to connect the extension and annealing zones. Holes threaded for different screw sizes were incorporated to permit fine tuning of the temperature profile. An air gap was left between the blocks in our experiments, but a layer of insulation may be used to provide better structural support to the block assembly. Despite its simplicity, this design offers a surprising amount of flexibility to regulate the temperature of each zone through proper selection of the screw materials, sizes, and the number of screws used.

A basic temperature control circuit was built to regulate the temperature (Supplementary Figure 5). This simplified and low cost homebuilt temperature control unit shares same power supply as the heating element and consumes minimal battery power for its operation. An initial calibration step is required to define the temperature set point, which involves using a secondary thermocouple sensor to detect the temperature and varying the potentiometer setting until the desired output temperature is reached (95 °C in this case). This on/off type controller works on the Wheatstone bridge principle such that as soon as the resistance of the probe thermistor equals the preset resistance of the potentiometer (corresponding to the block temperature), no current flows through the comparator (LM339) and the output circuit shuts off current to the heating element. When the temperature of the block drops below the set point, the circuit again turns on allowing heater to maintain the denaturing block at the desired temperature. While more sophisticated control circuits can be used, many of these approaches operate by redirecting part of the battery power through a parallel channel. Our on/off actuation scheme, on the other hand, is beneficial because deactivating the output circuit allows a considerable amount of battery power to be conserved over the duration of the PCR reaction.

We would like to emphasize that the device configurations reported here were chosen largely for simplicity in order to allow us to straightforwardly illustrate the basic concepts of

convective thermocycling. A variety of more sophisticated adaptations are possible depending on the needs associated with a particular application. We have arrived at an approximate figure of $10 (US) for the cost of the convective thermocycler device shown in Figure 4b as follows: $2 for two rechargeable AA batteries; $2 for the aluminum blocks, screws, heater assembly, and tubing; and approximately $6 for the temperature controller (when assembled on a small PC board).

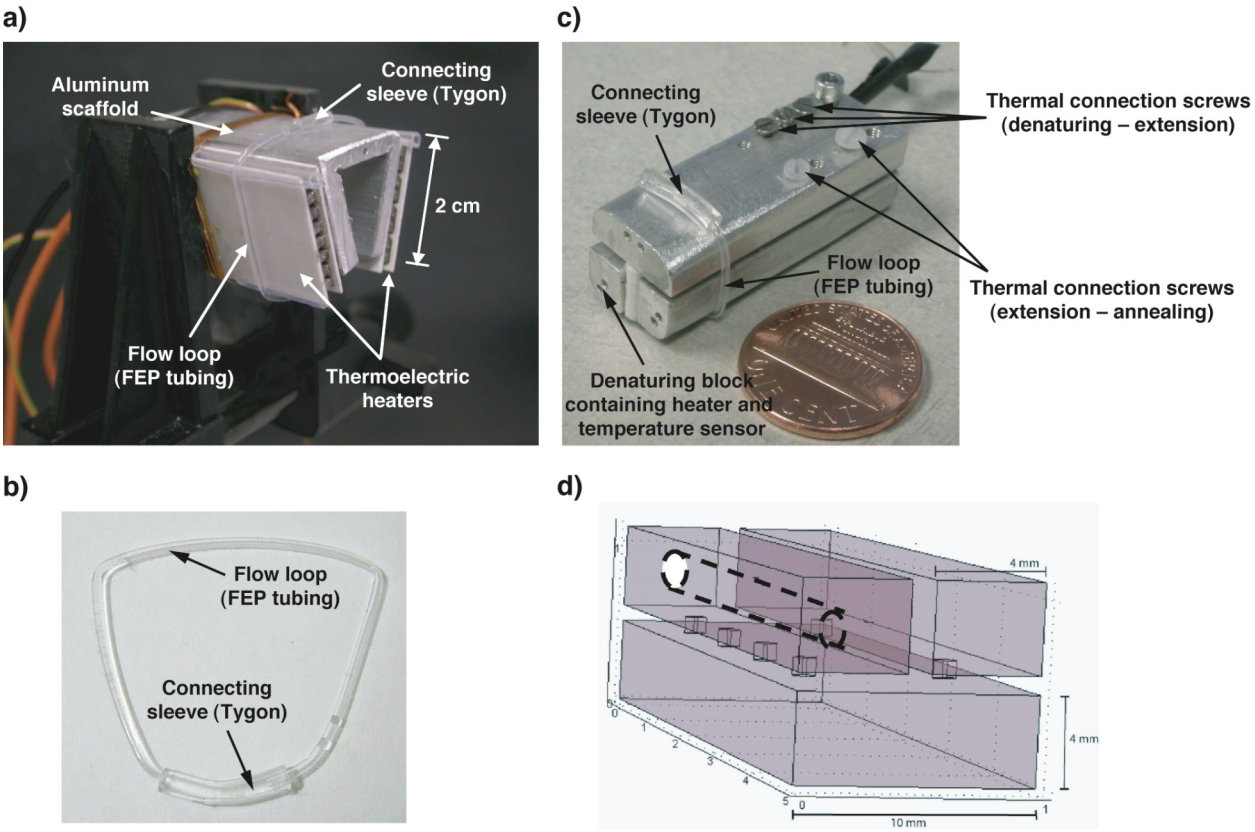

Supplementary Figure 4. Photographs of assembled convective thermocyclers. a) Triangular geometry incorporating a 9 cm long triangular loop mounted on a scaffold containing two independently controlled thermoelectric heaters. Note that the Tygon segment is shown on the top surface of the loop for display purposes; it would normally be located at the bottom (apex) of the loop to run the reaction. b) Photograph of an assembled flow loop. c) Pocket-sized thermocycler design consisting of a 5.5 cm long flow loop mounted around three aluminum blocks that are thermally interconnected using screws of different thermal conductivity. Note that the device is shown upside down for display purposes; the long (extension) zone side would normally at the bottom surface as illustrated schematically in Figure 2a. d) Detailed illustration of interconnected 3 block thermocycler design.

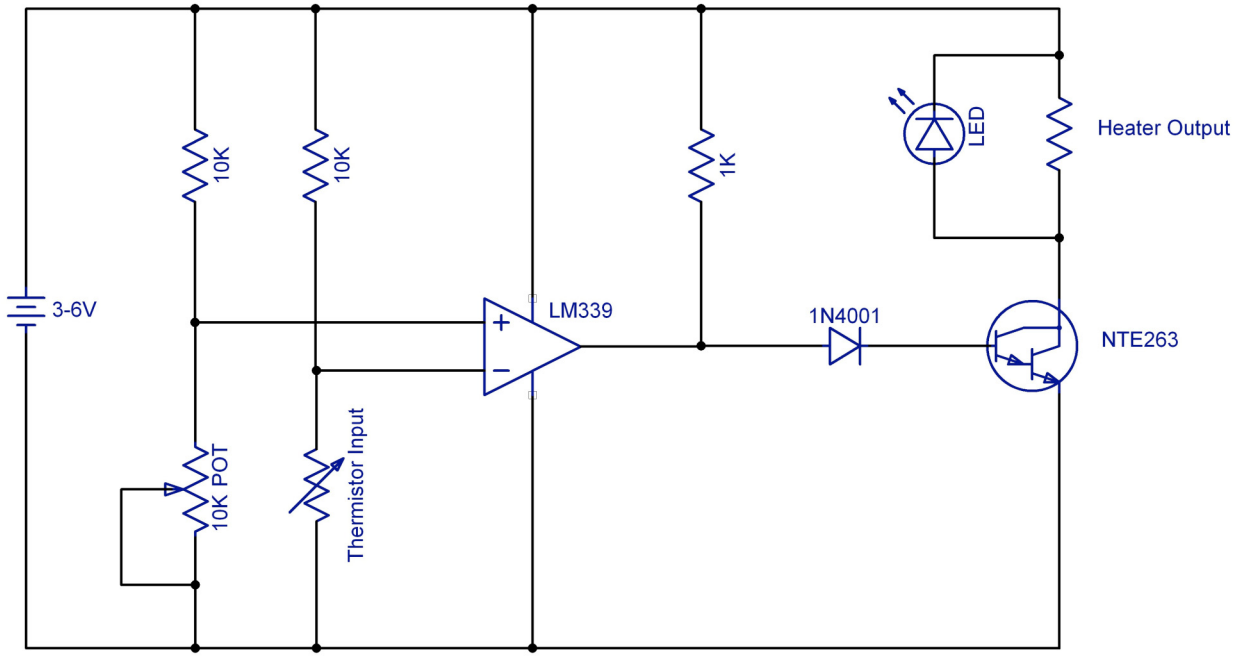

Supplementary Figure 5. Schematic diagram of the temperature control circuit employed in the battery powered thermocycler shown in Supplementary Figure 4c.

Analysis of laminar flow in convective loops

Appropriate scaling parameters for closed loop convective flows can be identified by considering a one-dimensional analysis of the steady-state mass, momentum and energy balances for a loop of length L and constant cross-sectional area A. [S1] The loop is oriented parallel to the vertical plane with different segments along the loop path maintained at different temperatures. Fluid density is assumed to remain constant except in the buoyancy term where a linear temperature dependence is imposed (i.e., the Boussinesq approximation $\rho = \rho_0 [1-\beta(T-T_0)]$, where ρ_0 and T_0 are reference density and temperatures respectively). A spatial coordinate 's' is defined extending counterclockwise along the length of the loop starting from an arbitrary origin. We also assume that fluid velocity u and temperature T remain constant across any cross-section of the loop.

In a closed loop with constant cross sectional area, conservation of mass implies that the fluid velocity u will also be constant along the length of the loop. In this case, viscous effects can be accounted for by postulating a linear relationship between wall shear stress τ_w and the mean fluid velocity $\tau_w = \alpha u$. For simplicity, we take as an estimate $\alpha = 8\mu/D$ where μ is the Newtonian coefficient of viscosity and D is the tube diameter (i.e., from the relationship for Poiseuille flow, although it is strictly not the case here). The steady-state momentum balance can then be integrated around the loop to yield

$$\frac{P\alpha}{\rho_0 A} u = \frac{\beta}{L} \int_0^L T(s)\tilde{g}(s)ds \qquad (1)$$

where P is the loop perimeter, $\tilde{g}(s) = g\cos(\theta)$ is the local component of gravity along the s direction, and β is the fluid's coefficient of volumetric expansion.

The steady-state energy balance over a control volume of fluid inside the loop can be expressed in a similar manner to yield

$$u\frac{\partial T}{\partial s} = \frac{q}{\rho_0 A C_p} + \frac{k}{\rho_0 C_p}\frac{\partial^2 T}{\partial s^2} \tag{2}$$

where q is the rate of heat gain per unit length of the loop, k is the fluid's coefficient of thermal conductivity, and C_p the fluid's specific heat at constant pressure. This expression is further simplified by (i) neglecting axial heat conduction (i.e., the second term on the right hand side of equation (2)), and (ii) assuming predominantly convective heat exchange between the fluid and tubing walls maintained at constant temperature T_w such that $q = hP(T - T_w)$, where h is a convective heat transfer coefficient. Substituting into equation (2) then yields

$$u\frac{dT}{ds} = \gamma[T - T_w(s)] \tag{3}$$

where the parameter $\gamma = -hP/\rho_0 AC_p$. Equations (1) and (3), along with appropriate boundary conditions, can then be evaluated to determine the fluid velocity associated with convective flow in a loop where different segments are maintained at different temperatures.

For simplicity, we consider the case of a square loop of length L composed of two vertical segments and two horizontal segments (Supplementary Figure 6) each maintained at a constant wall temperature (point 'A' is arbitrarily assigned as the origin). First, equation (3) is evaluated individually along each leg of the square loop subject to continuity of temperature at points A, B, C and D, and the results are combined to yield

$$T_D - T_B = \frac{\left[\left(T_{W2} - T_{W4}\right)e^{-\gamma L/4u} + \left(T_{W3} - T_{W1}\right)\right]\left[1 - e^{-\gamma L/4u}\right]}{1 + e^{-\gamma L/2u}}. \tag{4}$$

Next, equation (1) is evaluated along each leg, noting that terms associated with the horizontal legs for which $\theta = 90°$ (and hence $\cos(\theta) = 0$) make no contribution and can be neglected.

Substituting the result in equation (4) yields an equation for the fluid velocity u in terms of the loop geometry and wall temperatures imposed along each leg.

$$u = \frac{\beta \rho_0 A \tilde{g}}{P \alpha L}\left[\underbrace{\frac{L}{4}\left(T_{W2} - T_{W4}\right)}_{Term-1} + \underbrace{\frac{u}{\gamma}\left(e^{-\gamma L/4u} - 1\right)\left\{ \frac{\left[\left(T_{W2} - T_{W4}\right)e^{-\gamma L/4u} + \left(T_{W3} - T_{W1}\right)\right]\left[1 - e^{-\gamma L/4u}\right]}{1 + e^{-\gamma L/2u}} + T_{W2} - T_{W4} \right\}}_{Term-2} \right] \tag{5}$$

Substituting characteristic numerical values of the corresponding parameters relevant for the conditions of interest in PCR thermocycling reveals that the magnitude of Term-2 is small compared with Term-1, so that equation (5) can be approximated as

$$u \approx \frac{\beta \rho_0 A \tilde{g}}{P \alpha L} \frac{L}{4}\left(T_{W2} - T_{W4}\right). \tag{6}$$

Simplifying in terms of common geometric and fluid properties yields the scaling

$$u \propto \frac{\beta \tilde{g} D^2 \Delta T}{\nu}. \tag{7}$$

Recalling the definition of Rayleigh number

$$Ra = \frac{\tilde{g} \beta \Delta T D^3}{\nu \kappa} \tag{8}$$

equations (7) and (8) can be combined to yield the following scaling

$$u \propto Ra \frac{\kappa}{\nu} \tag{9a}$$

or equivalently

$$Ra \propto \frac{uD}{\kappa}. \tag{9b}$$

Finally, substituting $u = L/t$ yields a scaling for the cycle time (i.e., the time for a fluid element to travel along the entire length of the loop).

$$t \propto \frac{LD}{\kappa Ra} \tag{10}$$

An interesting observation is that, although this analysis has considered the case of a rectangular loop geometry, the scalings obtained for velocity and cycle time should be generally applicable to loop configurations that are symmetric about a vertical centerline. This is supported by the results of computational flow simulations for two additional symmetric triangular loop geometries (θ = 15 and 60°) where the total loop length L kept fixed at 9 cm as in the θ = 30° triangular configuration used to perform PCR (Figure 1a). It can be seen that data for all three geometries collapse onto a master curve consistent with the expected scaling (Supplementary Figure 7).

Reference

[S1] Agrawal, N. (2006) *Ph.D. Dissertation*, Texas A&M University, Chapter 5.

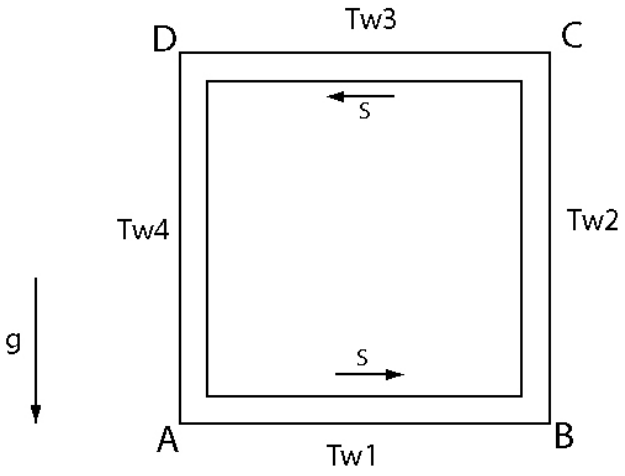

Supplementary Figure 6. Schematic of a square convective flow loop geometry. Point 'A' is the arbitrary origin and spatial coordinate *s* extends from 'A' in counterclockwise direction. The loop has a total length *L*, with equal segments of length *L*/4. Each segment is maintained at a constant wall temperature $T_{w,i}$.

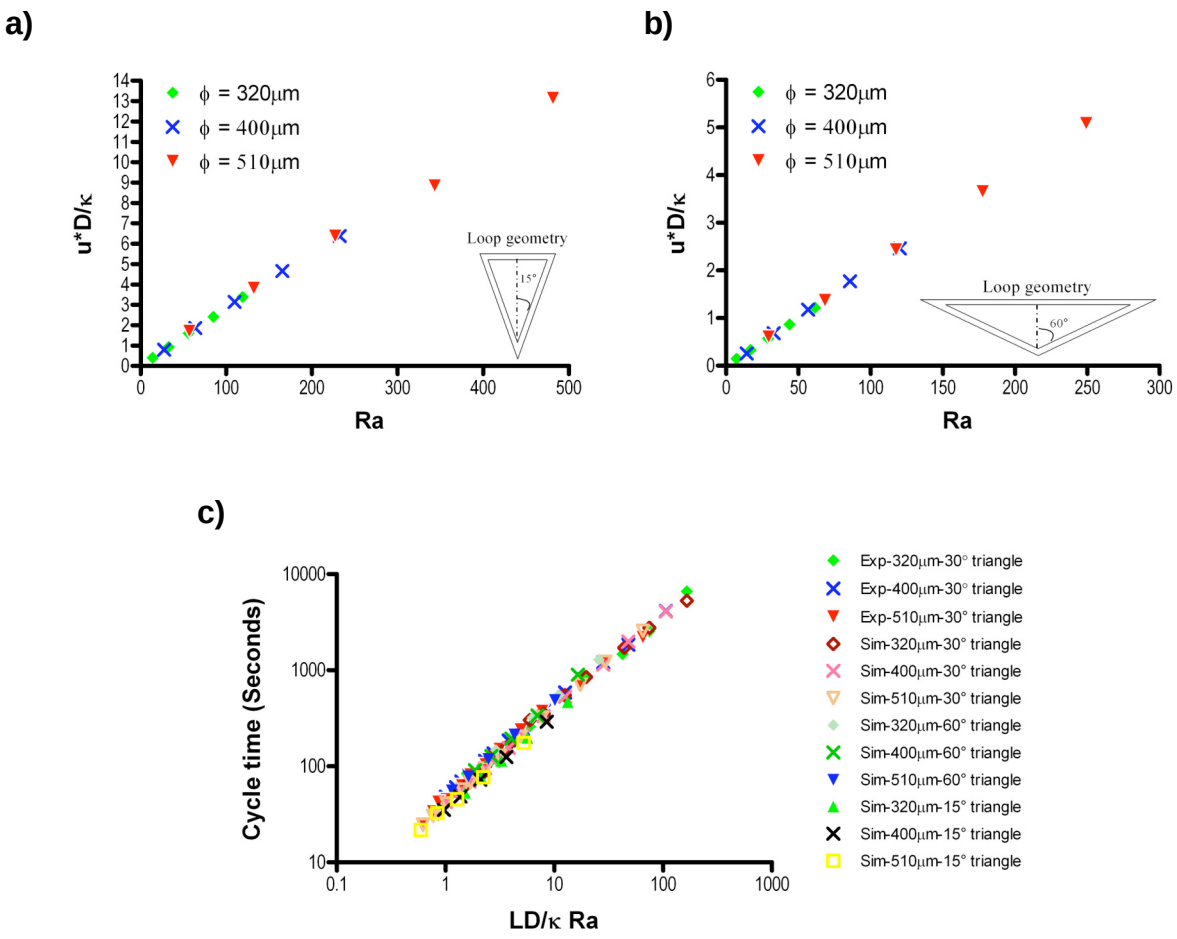

Supplementary Figure 7. Flow parameter scalings for additional triangular convective flow loop geometries. a-b) Results of computational flow simulations in 9 cm long triangular loops with three different diameters expressed in terms of the parameter uD/κ versus Rayleigh number. Symmetric loops with vertical segments oriented at a) θ = 15°, and b) θ = 60° were analyzed. c) These results superimpose with the corresponding experimental and computational data for the θ = 30° loop used to perform PCR.

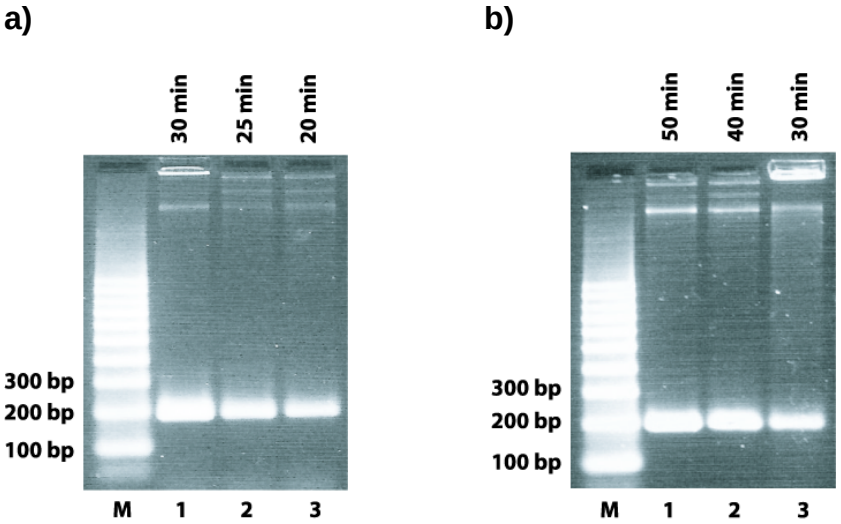

Supplementary Figure 8. Amplification as a function of reaction time for a 191 bp target associated with membrane channel proteins M1 and M2 of the influenza-A virus. Lane M: 100 bp marker, lanes 1-3: amplification products after various reaction times (indicated at the top of each gel image) in reactor volumes of a) 16 μL (400 μm dia., 69 s cycle time), and b) 10 μL (320 μm dia., 102 s cycle time).

Supplementary Table 1. PCR primer sequences employed for various targets studied.

	Sequence	T_m (F/R) (°C)	Name	Amplicon Size
F-PCR R-PCR	5'-GTCACCAGTGCAGTGCTTGATAACAGG-3' 5'-GATGACGCATCCTCACGATAATATCCGG-3'	70.9 / 73.2	1.3kb fragment of λ DNA	1.3k bp
F-PCR R-PCR	5'-ACGGCCGAGCGGAAATCGT- 3' 5'-CTGCTTGCTGATCCACATCT- 3'	59 / 59	Human β-Actin	474 bp
F-PCR R-PCR	5'-GGCACCAGTCAGACCGATATGT-3' 5'-ATTGTGAGCGATCTCGGCACAG-3'	67 / 71	Human L32	242 bp
F-PCR R-PCR	5'-GCAGCGTAGACGCTTTGTCCAAAAT-3' 5'-CAGCCCCCATCTGTTGTATATGAG-3'	68 / 67	Influenza A virus	191 bp
F-PCR R-PCR	N/S	 70 / 71 70 / 71 67 / 68 69 / 70 69 / 70	*Multiplex PCR including:* Rhino virus Adenovirus Influenza virus Corona virus Respiratory syncytial virus	 547 bp 484 bp 390 bp 315 bp 246 bp

F-Forward, R-Reverse, N/S-sequences not supplied by the vendor